crystals

MDPI

Article

Amorphous-like TiN Films as Barrier Layers for Copper

Shicheng Han [1], Shicheng Yang [1], Xiaohong Zeng [1], Ying Wu [1], Tong Liu [2], Hu Wang [2] and Sunan Ding [1,*]

[1] School of Integrated Circuits, Nanjing University, Suzhou 215163, China; 522022000004@smail.nju.edu.cn (S.H.); 522022000016@smail.nju.edu.cn (S.Y.); 602023730005@smail.nju.edu.cn (X.Z.); ywu2023@nju.edu.cn (Y.W.)

[2] Vacuum Interconnected Nanotech Workstation (Nano-X), Suzhou Institute of Nano-Tech and Nano-Bionics, Chinese Academy of Sciences, Suzhou 215123, China; tliu2015@sinano.ac.cn (T.L.); hwang2016@sinano.ac.cn (H.W.)

* Correspondence: dingsunan@nju.edu.cn

Abstract: The titanium nitride (TiN) columnar structure results in a rapid diffusion of copper atoms into the substrate along a vertical path. In this paper, the TiN columnar growth process was modified, which resulted in the deposition of amorphous-like films. The amorphous-like TiN layer demonstrated a low resistivity of 75.3 μΩ·cm. For the test structure of Cu/TiN/SiO_2, the Cu diffusion depth in the 3 nm TiN middle layer was only approximately 1 nm after annealing at 750 °C for 30 min. Excellent copper diffusion barrier due to high density and complex diffusion pathways. The results of this study suggest that conventional barrier materials can still be used in ultra-narrow copper interconnects.

Keywords: metallization; diffusion; amorphous-like; titanium nitride; barrier

Citation: Han, S.; Yang, S.; Zeng, X.; Wu, Y.; Liu, T.; Wang, H.; Ding, S. Amorphous-like TiN Films as Barrier Layers for Copper. *Crystals* **2024**, *14*, 951. https://doi.org/10.3390/cryst14110951

Academic Editor: Francisco M. Morales

Received: 30 September 2024
Revised: 10 October 2024
Accepted: 11 October 2024
Published: 31 October 2024

1. Introduction

The electrical resistance of interconnect wires increases with decreasing size, causing signal delay and energy consumption, which limits further downscaling of integrated circuits. The width and resistivity of interconnect wires, consisting of copper and diffusion barriers, must shrink [1]. The conventional barrier material, tantalum nitride (TaN), fails at thicknesses below 3 nm [2,3]. The diffusion barrier performance of the TiN film is inferior to TaN due to its more vertical columnar structure [4,5]. The columnar crystal structures in the traditional barrier layer form the main pathways of Cu atom diffusion [6], as depicted in Figure 1.

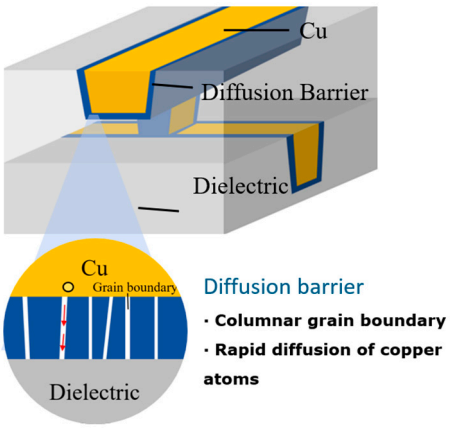

Figure 1. Schematics of copper interconnect cross-section and copper diffusion channels.

Several new materials have been the subject of extensive research to improve vertical diffusion, for example, 2D materials [7–9], SAM [10], and HEAs [11]. Nevertheless, novel barrier material preparation processes hinder the integration of current interconnect technologies. Improving the columnar structure of traditional barrier materials to meet the requirements for nano-scale processes is crucial, given their compatibility with existing silicon manufacturing standards [12–14].

Reactive sputtering is commonly used to deposit metal nitride films from metal targets in N_2 or N_2/Ar mixtures. However, this kind of TiN film formed preferentially with a columnar microstructure due to the presence of N_2 and N_2^+ [15,16]. Gall et al. have explained this effect based on density functional theory and further indicated that excess N atoms enhanced the surface island nucleation rate [17]. So, it is understandable that fast deposition of TiN film by reactive sputtering results in more grain boundaries in the columnar crystals, which makes Cu diffusion feasible.

Here, we provide an approach that converts TiN, a low resistivity liner material, to an amorphous-like material to serve as an ultrathin diffusion barrier. This kind of phase is called amorphous-like because the crystallite size and X-ray diffraction (XRD) features are typical of an amorphous material, but a short-range order is still visible. Note that this paper is the first to demonstrate that TiN can be prepared by growing amorphous-like rather than columnar. An extended structure zone model provides a qualitative theoretical basis for amorphous-like phase formation [15,18] through the employment of an ultra-high-vacuum (UHV) magnetron sputtering system to obtain a near-ideal growing environment. Additionally, in order to circumvent the nitrogen-promoted columnar growth of TiN [19], a direct sputter deposition technique with a titanium nitride target and pure argon was used. Details of the growth are in our other unpublished article.

In this work, we focused on the diffusion properties of copper in the amorphous-like TiN films. Extremely low copper diffusion rates indicate that amorphous-like structures do not have fast diffusing pathways. Ultra-thin structures, low resistivity, high thermal stability, and compatible processes show their advantages as effective diffusion barriers.

2. Experimental

After installation of the TiN target, the chamber was baked and degassed to achieve ultra-high vacuum pressures ($<10^{-9}$ Torr). Prior to film deposition, the target was pre-sputtered to remove surface oxidation and contamination. TiN thin films were deposited at a substrate temperature of 400 °C and sputtering power of 60 W, with the target positioned 15 cm from the substrate. The vacuum was maintained at 2×10^{-3} Torr during growth. Silicon substrates coated with SiO_2 were used, pre-cleaned by ultrasonication in acetone and isopropanol. For process optimization, 26.5 nm thick TiN film was first prepared at a low deposition rate of 1.33 nm/min.

The chemical composition of as-deposited TiN films was characterized using an X-ray photoemission spectroscope (XPS, ESCALAB Xi+, Thermo Fisher, Waltham, MA, USA). The morphology and microstructure were examined using transmission electron microscopy (TEM, HT-7700, Hitachi, Tokyo, Japan) and scanning electron microscopy (SEM, Scios, FEI, Hillsboro, OR, USA). X-ray diffractor (XRD, D8 Advance, Bruker AXS, Billerica, MA, USA) was employed to analyze the crystallization, and atomic force microscopy (AFM, MFP-3D, Oxford Instruments, Oxford, England) measured surface roughness. Film thickness was determined by an ellipsometer (iSE, J.A. Woollam, Lincoln, NE, USA), and sheet resistance was measured using a four-point probe (Cresbox, Napson Corp, Tokyo, Japan).

Thermal stability tests were conducted using a self-developed rapid thermal annealing furnace (RTA). The ability of TiN films to block Cu diffusion and their thermal stability was further investigated using a multi-layer structure Cu(100 nm)/TiN(3 nm)/SiO_2/Si. For comparison, a Cu/SiO_2/Si structure without the TiN intermediate layer was prepared under identical conditions.

Samples underwent annealing in an RTA furnace filled with pure nitrogen at approximately 3.5×10^{-4} Torr. The annealing process involved a ramp-up heating rate

of 50 °C/min, followed by 30 isothermal annealing for 30 min at each temperature step ranging from 200 °C to 800 °C.

3. Result and Discussions

3.1. Chemical Composition

Carbon C1s were used to remove any possible shift in the binding energy due to sample charging. In Figure 2a,b, the core level spectra of Ti 2p and N 1 s in the TiN films are analyzed to reveal their chemical states [20]. The Ti 2p spectrum (Figure 2a) exhibits characteristic peaks corresponding to Ti 2p3/2 and Ti 2p1/2 with binding energies of 454.8 eV and 460.8 eV, respectively, indicating spin-orbit splitting in TiN. A satellite peak at 457.6 eV, attributed to TiN, is observed, consistent with the literature findings on TiN films [21]. Additionally, due to the oxidation of the target, weaker components associated with titanium oxide (TiO_2) and titanium oxynitride (TiO_xN_y) are discerned at binding energies of 458.4 eV and 456.1 eV, respectively.

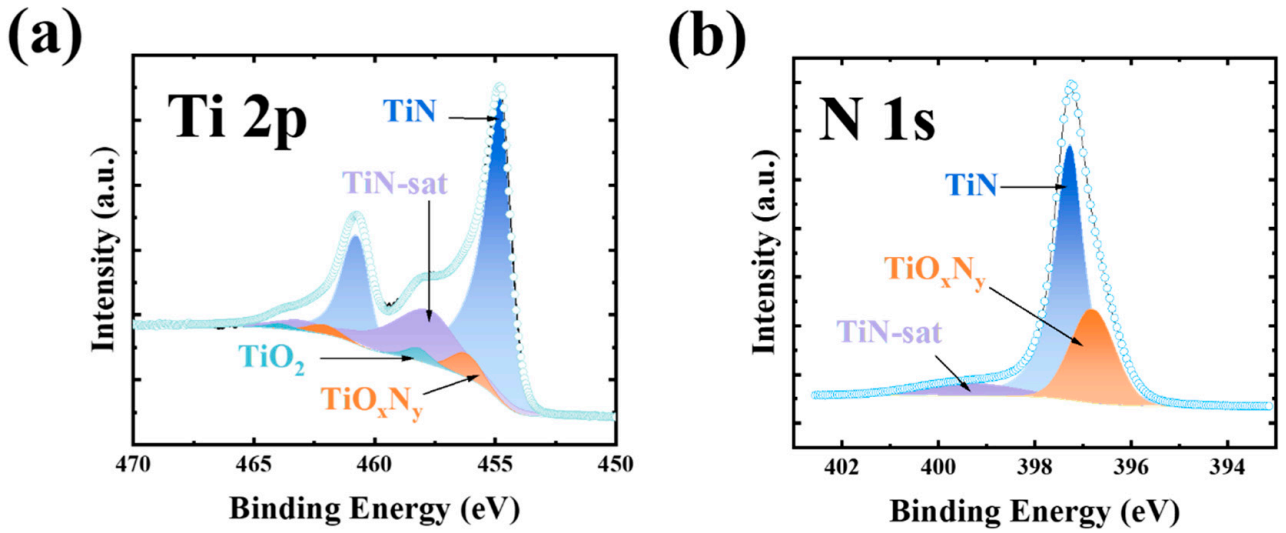

Figure 2. XPS core level spectra of TiN (**a**) Ti 2 p, (**b**) N 1 s.

The N 1 s spectrum (Figure 2b) reveals a dominant peak centered at 397.3 eV, corresponding to nitrogen in TiN, along with a minor peak at 397.0 eV attributed to nitrogen in TiO_xN_y.

The above results show that the core-level binding energies of the TiN film prepared by direct sputtering are in good agreement with published data, and the atomic ratio of titanium to nitrogen is approximately 1.05 [22,23]. Previous studies have highlighted that maintaining a stoichiometric ratio in TiN is critical for its impermeability properties, as Cu impurity diffusion is significantly hindered in stoichiometric TiN compared to non-stoichiometric compositions [24].

Microstructure. The transmission electron microscopy (TEM) cross-sections presented in Figure 3a,c clearly reveal lattice fringes with varied orientations, indicating the absence of preferential orientation in the TiN films deposited by the direct sputtering of a TiN target. Figure 3b shows the corresponding fast Fourier transform (FFT) pattern extracted from the region marked by the red dashed box in Figure 3a. The pattern exhibited bright dots and rings, characteristic of nanocrystalline and amorphous films with diverse crystallographic orientations. The lattice parameters are determined to be 0.245 nm for TiN (111) and 0.212 nm for TiN (200). Figure 3d provides an enlarged view of the area highlighted by the yellow box in Figure 3c, clearly depicting the amorphous structure. The FFT results shown in Figure 3e further confirm the amorphous nature of this region.

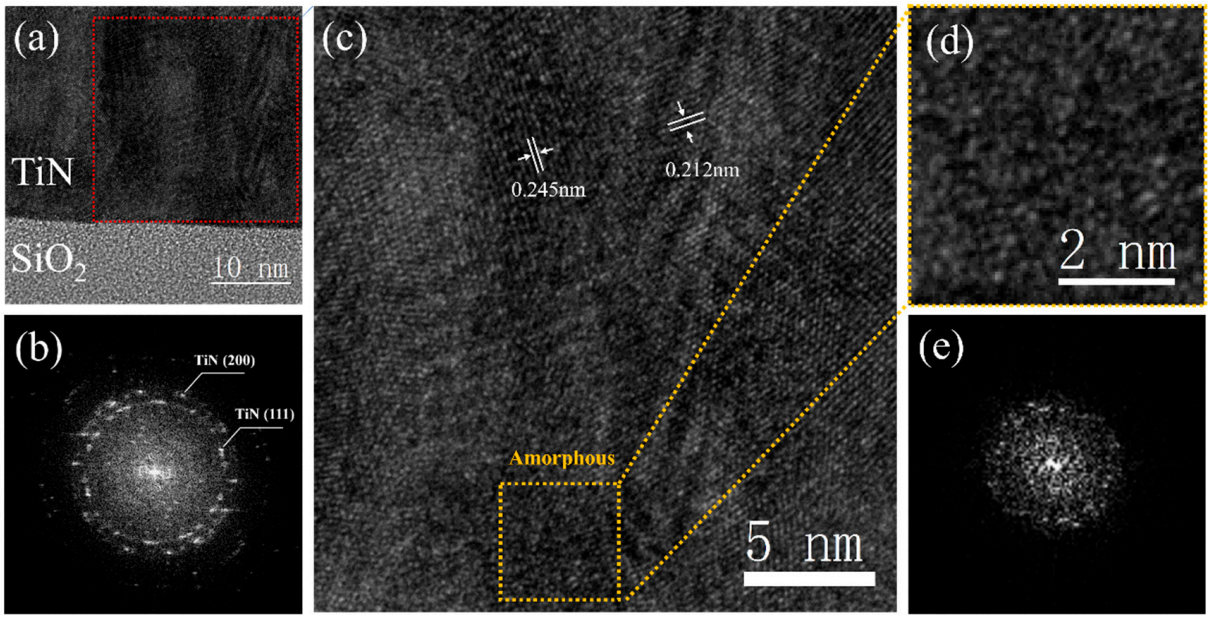

Figure 3. (**a**) Low-magnification TEM image of TiN. (**b**) FFT from the red dashed box of the TEM image. (**c**) High-resolution TEM image. (**d**) Magnification of the area indicated by the yellow box in (**c**). (**e**) FFT results for the area depicted in (**d**).

Importantly, the amorphous-like structure significantly increased the diffusion path for Cu atoms within the TiN thin films, owing to its complex grain boundary structure. This characteristic is crucial to enhance the barrier properties of TiN against Cu diffusion, which is essential for maintaining the integrity and reliability of advanced semiconductor devices. Further studies focusing on the interface properties, thermal stability, and long-term performance under operational conditions will be necessary to fully exploit the potential of amorphous-like TiN films in practical applications.

Film roughness and mass density are also key indicators for evaluating the performance of TiN as a diffusion barrier. The atomic force microscopy (AFM) image in Figure 4 shows the surface morphology of the TiN films. The root-mean-square (RMS) roughness of the 26.5 nm film measures 0.9 nanometers, which is comparable to the TiN films of similar thickness produced by atomic layer deposition (ALD) methods [25]. Even smoother surfaces are observed for thinner TiN layers (Figure 4b) prepared under identical conditions.

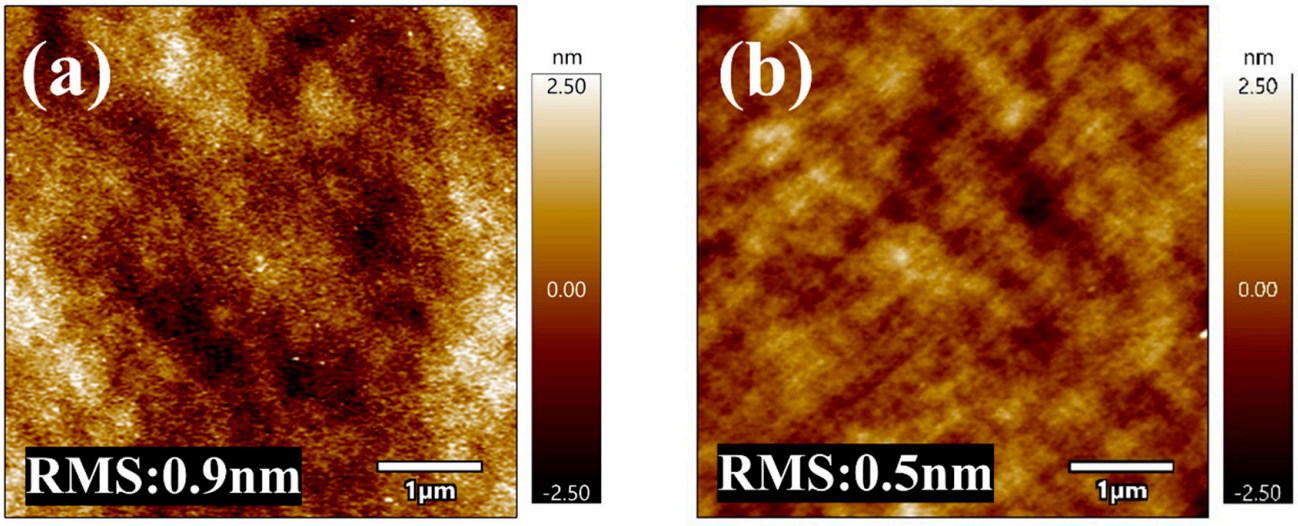

Figure 4. AFM micrographs of TiN films with different thickness: (**a**) 26.5 nm. (**b**) 3 nm.

Figure 5a shows the X-ray diffraction (XRD) patterns of the sputtered TiN films alongside the substrate, with the relative peak positions of the (111) and (002) reflections referenced to JCPDS card #38-1420 also plotted as a reference. These patterns demonstrated the amorphous nature of the prepared TiN films.

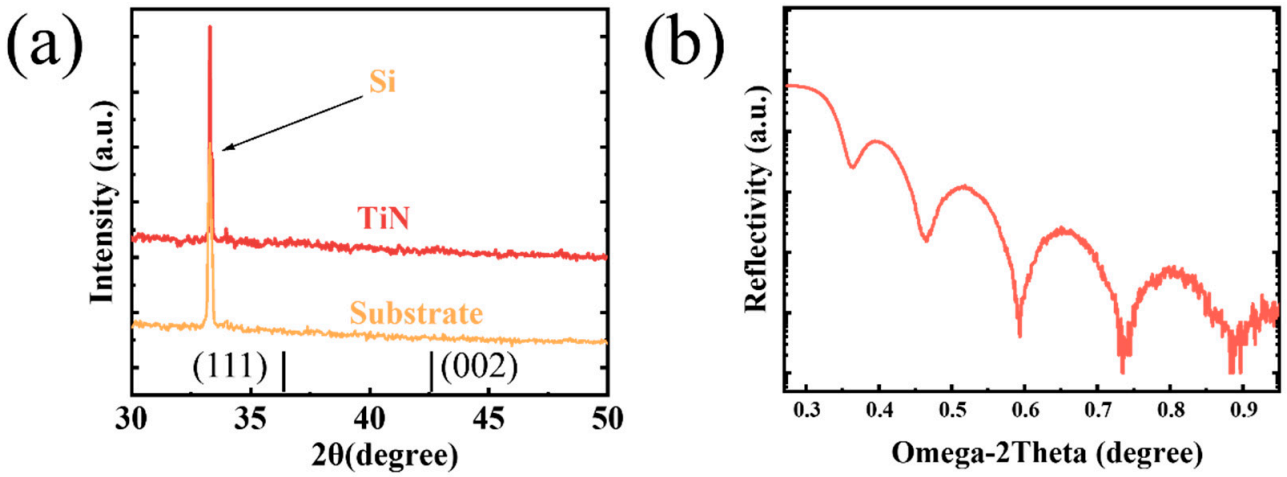

Figure 5. (**a**) XRD spectra of 26.5 nm TiN films and substrates. (**b**) XRR spectra for 26.5 nm TiN thin films.

Density characterization was performed using X-ray reflectivity (XRR), as shown in Figure 5b, employing the Omega-2Theta linked scanning mode and analyzed using AMASS software (Version 1.1). The XRR curve indicates a density of 5.79 g/cm^3 for the 26.5 nm thick TiN film. Variations in density ranging from 3.8 to 5.7 g/cm^3 have been reported for TiN thin films prepared by reactive sputtering [26–29].

The resistivity of the 26.5 nm and 3 nm thickness films were measured to be 75.3 μΩ·cm and 179.5 μΩ·cm, respectively, using the Four-point probe method. These values are at least six times lower than those reported for TaN [30]. The very smooth surface not only reduces the contact area between the Cu and TiN films but also reduces electron scattering at the interface, thereby lowering the interconnect resistance [25]. Consequently, this type of TiN film is anticipated to serve as an effective barrier against Cu diffusion, owing to its excellent properties of high mass density and very smooth surface.

3.2. Thermal Reliability

Figure 6a shows the X-ray diffraction (XRD) patterns of the Cu/SiO_2 samples annealed at various temperatures. For the as-deposited sample, only the Cu (111) and Cu (200) peaks were observed. As the annealing temperature increases, additional peaks corresponding to Cu_3Si (012) and Cu_3Si (300) emerge, indicating an enhanced interaction between Cu and SiO_2 layer [31]. In contrast, Figure 6b depicts a structure with a 3 nm TiN layer as a barrier. No Cu_3Si peaks are observed even after annealing up to 800 °C, indicating the effective blocking of Cu and Si diffusion across the TiN barrier layer.

Figure 7 shows the sheet resistance of the Cu layer in the Cu/TiN/SiO_2 film as a function of the annealing temperature. Up to 700 °C, there was a minimal change in resistance, but a sharp increase by three orders of magnitude was observed at 750 °C. Importantly, this increase in resistance cannot be attributed to the failure of the TiN barrier layer, as evidenced by the absence of Cu silicide formation at this temperature, as shown by the XRD results in Figure 6b.

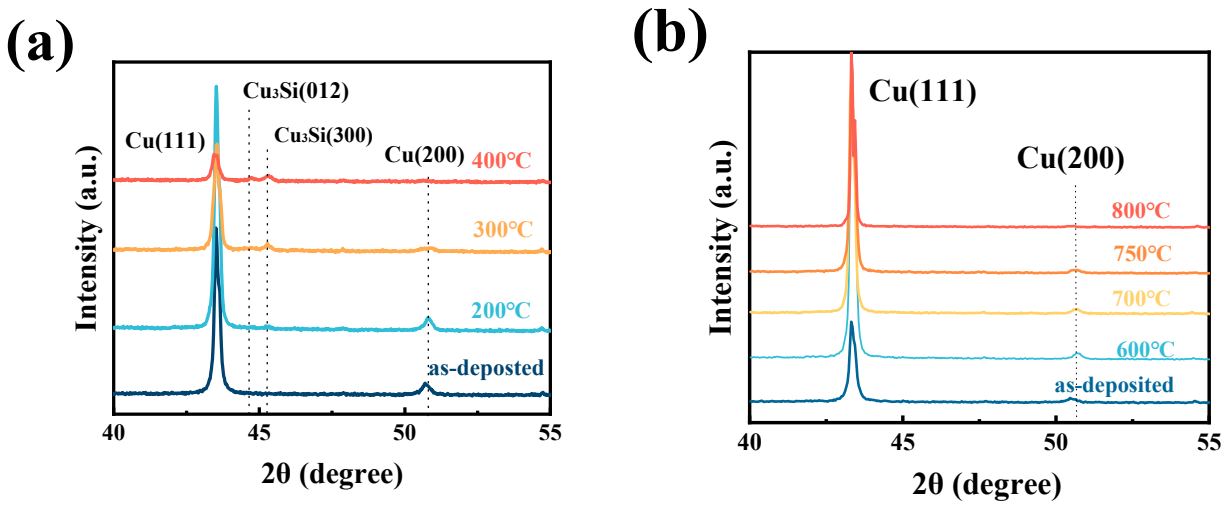

Figure 6. (**a**) XRD patterns of samples annealed at different temperatures for Cu/SiO_2; (**b**) the XRD patterns of the $Cu/TiN/SiO_2$ structure at different annealing temperatures.

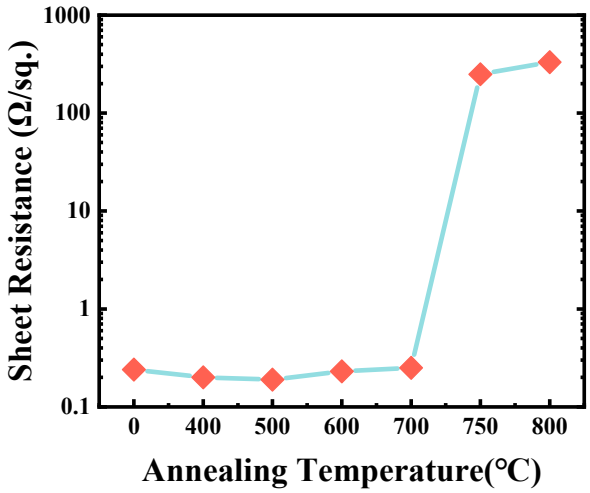

Figure 7. The resistance of the $Cu/TiN/SiO_2$ structures after annealing for 30 min at different temperatures.

To further investigate this phenomenon, the surface morphologies of the samples annealed at different temperatures were examined using scanning electron microscopy (SEM).

3.3. Variations in Microstructure

The surface microstructure of the as-deposited film appeared granularly and then transformed into large grains after annealing at 600 °C, as shown in Figure 8a,b, respectively. This transformation may be attributed to Cu recrystallization, a process typically occurring in the temperature range of 300–500 °C [32]. The surface roughness further increased after annealing at 700 °C, as shown in Figure 8c. When the temperature increases to 750 °C in Figure 8d, "Cu islands" are observed, indicating partial melting of Cu, leaving portions of the TiN layer uncovered and oxidized. Obviously, the sudden increase in the resistivity of the Cu sheet after annealing at 750 °C is, therefore, attributed to Cu melting rather than the formation of Cu silicide.

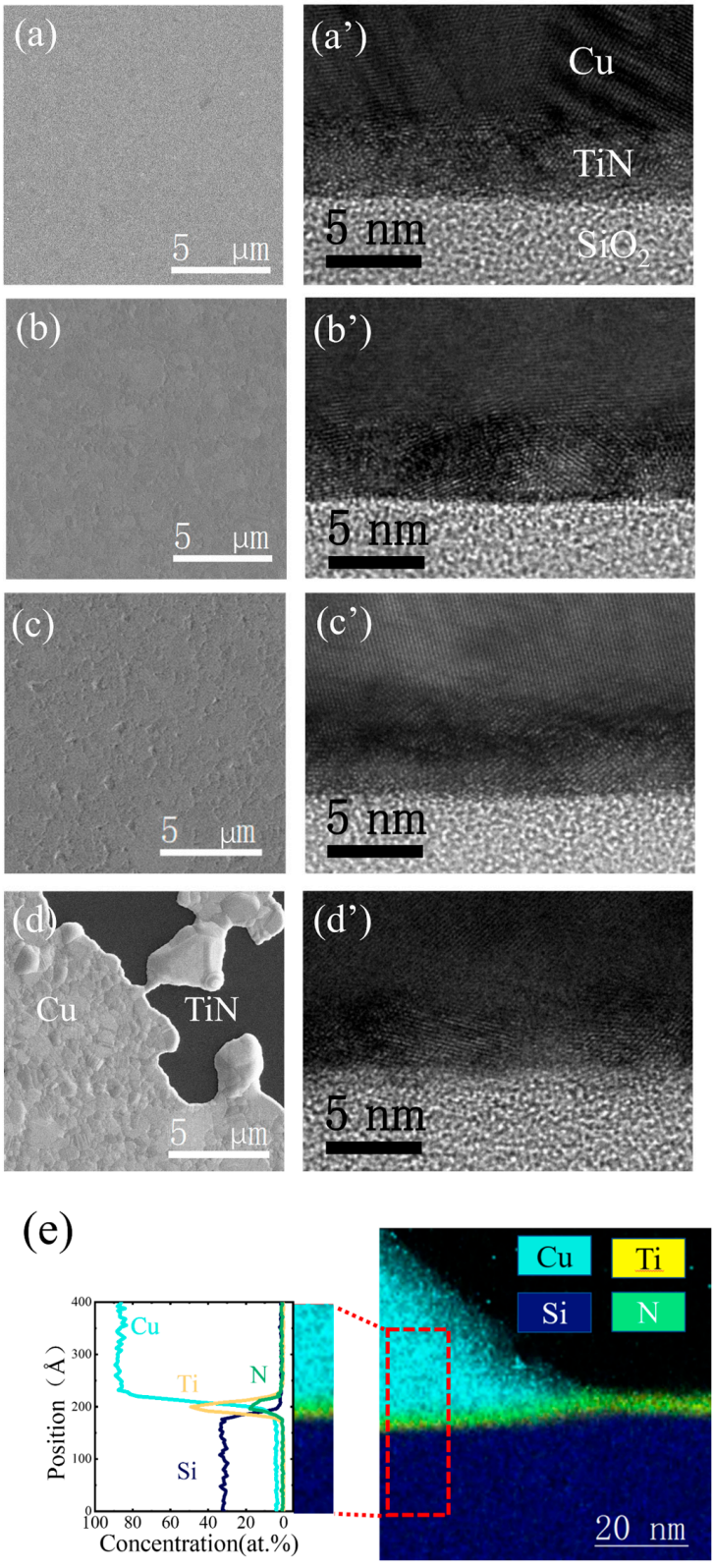

Figure 8. SEM micrographs on the Cu/TiN/SiO_2 surfaces and the corresponding cross-sectional TEM images for the samples of (**a**,**a′**) as-deposited, (**b**,**b′**) after 600 °C annealing, (**c**,**c′**) after 700 °C annealing; (**d**,**d′**) after 750 °C annealing; EDS patterns of the Cu/TiN/SiO_2 after 750 °C annealing (**e**).

Transmission electron microscopy (TEM) analysis was conducted on the Cu/TiN/SiO_2 samples to investigate the microstructures of the TiN interlayer and its interfaces with Cu

and SiO_2. In Figure 8a′, the as-deposited 3 nm thick TiN film exhibits an amorphous-like structure with very smooth interfaces between Cu/TiN and TiN/SiO_2. As the annealing temperature increases, as shown in Figure 8b′–d′, the TiN film undergoes a transformation from an amorphous-like to a nanocrystalline structure. Additionally, slight intermixing at the Cu/TiN interfaces is observed due to atomic diffusion across the interface under thermal stress. The mixing layer at the TiN/SiO_2 interface arises from the reaction between TiN and SiO_2, which is confined to the interface with negligible diffusion of Si atoms at high temperatures.

The qualitative indication of interfacial integrity is provided by EDS. The potential for errors in atomic content due to the EDS measurement method is not addressed in this paper. The composition distribution in the fringe region of the Cu agglomeration is presented in Figure 8e, characterized using energy dispersive spectroscopy (EDS), confirming the integrity of the TiN layer after annealing at 750 °C, with no evidence of copper diffusion across the barrier. The superiority of our study was demonstrated by comparing our results with the corresponding data from the previously published literature (Table 1).

Table 1. Results of different barriers from this work and as reported in the literature.

Source	Crystal Structure of Films	Failure Temperature (°C)	Annealing Condition	Ref.
Mo_2N (4 nm)	Amorphous-like	700	N_2, 30 min	[12]
W−Si−N (4 nm)	Amorphous	650	vacuum, 30 min	[13]
Graphene (1 nm)	2D	800	vacuum, 5 min	[33]
TiN (420 nm)	Polycrystalline	700	vacuum,1 h	[34]
CoWP (760 nm)	Amorphous	500	vacuum, 30 min	[6]
TiN (3 nm)	Amorphous-like	800	N_2, 30 min	This work

3.4. Diffusion Activation Energy

The copper diffusion mechanism can be explained by diffusion activation energy and rate. According to the EDS results, Figure 9a shows the elemental distributions of Cu and Si across the Cu/TiN/SiO_2 structures before and after thermal annealing. Notably, Cu diffusion at the interface intensifies notably with increasing annealing temperature. The diffusion distances of Cu through the barriers were determined by defining the interface position at 50% of the maximum atomic concentration. The diffusion distance (x) is governed by Fick's laws: $x = 2\sqrt{Dt}$, where D is the grain boundary diffusivity and t is the diffusion time. The activation energy (Q) for barrier diffusion can be determined from the equation: $D = D_0 \exp\left(-\frac{Q}{kT}\right)$, where D_0 is the intrinsic diffusion coefficient, k is the Boltzmann constant, and T is the temperature.

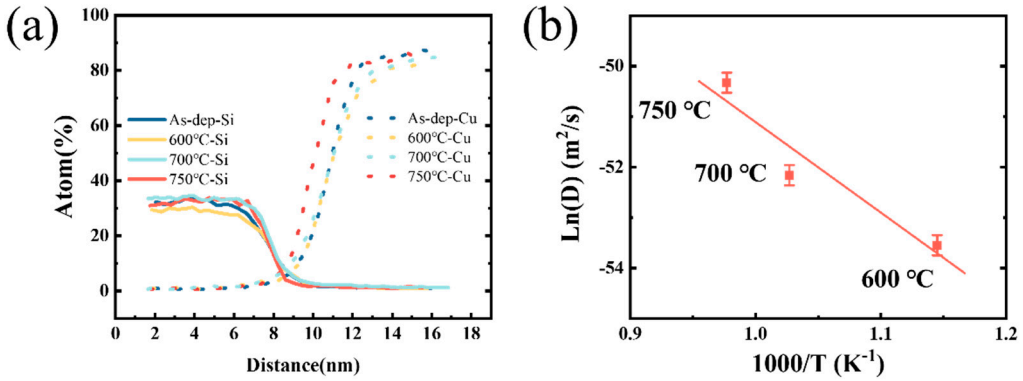

Figure 9. (**a**) Elemental concentration distribution of Cu and Si in film after thermal annealing at 600 °C and 750 °C. (**b**) Diffusivities of Cu in thermally annealed Cu/TiN/SiO2 film stacks at 600~750 °C.

Figure 9b plots the correlation between ln (D) and 1/T, allowing for the assessment of the Cu diffusion activation energy (Q) in TiN from the slope of the linear fit. The value of Q and D_0 were inferred to be 1.3 ± 0.2 eV and (2.8 ± 1.3) × 10^{-15} m^2/s, respectively, and compared with corresponding data from the previous literature, as summarized in Table 2.

Table 2. Results of diffusion activation energy and rate from this work and as reported in the literature.

Material	Calculation Method	D_0(m^2/s)	Q (eV)	D (m^2/s) (700 °C)	Source
TiN	Experiment	6.4×10^{-15}	0.29	-	[35]
TiN	Theory	-	0.77~1.2	-	[24]
TaN	Experiment	-	-	7.8×10^{-18}	[36]
$TaN_{0.7}$	Experiment	1.3×10^{-9}	1.16	1.2×10^{-15}	[37]
HEA (TiTaCrZrAlRu)	Experiment		1.66	1.6×10^{-21}	[11]
TiN	Experiment	(2.8 ± 1.3) × 10^{-15}	1.3 ± 0.2	2.2×10^{-23}	This work

An early experimental study obtained a migration activation energy Q of 0.29 eV for Cu diffusion in columnar TiN [35]. Copper lattice diffusion activation energies in stoichiometric and nonstoichiometric TiN are 4.5 eV and 2.7 eV, respectively [24]. The activation energy of defect diffusion is approximately half of that of the lattice diffusion. In our work, the atomic ratio of titanium to nitrogen is about 1.05, and the diffusion activation energy of 1.3 ± 0.2 eV is a reasonable value. The directly sputtered TiN film in this study exhibits the lowest intrinsic diffusion coefficient and highest diffusion activation energy reported to date, indicating significantly enhanced Cu diffusion blocking capability of the TiN barrier.

4. Conclusions

In this paper, amorphous-like TiN thin films are prepared and characterized. Copper diffusion is greatly hindered by dense amorphous-like structures. The sudden increase in the resistivity of the Cu sheet after annealing at 750 °C is attributed to surface morphology changes. The experimentally determined parameters (e.g., diffusion distance, annealing temperature, diffusion time) were used to calculate the values of the diffusion activation energy, and the results indicate that copper diffuses through defects rather than through columnar grain boundaries. The diffusion diffusivity of Cu through this TiN barrier is estimated at 2.2 × 10^{-23} m^2/s, markedly lower than other published values for grain boundary diffusion, attributed to the absence of vertical diffusion paths within the thin film.

The present work indicated that the amorphous-like TiN films have excellent process compatibility, ultrathin structures, low resistivity, and excellent copper diffusion-blocking capabilities. Amorphous-like TiN films can be used as barrier material for advanced technology nodes.

Author Contributions: Conceptualization, S.H., S.Y., and Y.W.; data curation, S.H., S.Y., and T.L.; formal analysis, S.H., S.Y., X.Z., T.L., and H.W.; investigation, S.H., S.Y., and H.W.; methodology, S.H., S.Y., and X.Z.; software, S.H.; validation, S.Y. and X.Z.; writing–original draft, S.H.; writing—review and editing, Y.W. and S.D.; project administration, S.D.; supervision, Y.W. and S.D.; funding acquisition, S.D. All authors have read and agreed to the published version of the manuscript.

Funding: This research was funded by the National Natural Science Foundation of China (NNSFC) (Grant No. 62174171).

Data Availability Statement: Data will be made available upon request.

Acknowledgments: The authors acknowledge the technical support from Nano-X from Suzhou Institute of Nano-Tech and Nano-Bionics, Chinese Academy of Sciences (SINANO). The authors would like to express their sincere gratitude to the Interdisciplinary Research Center for Future Intelligent Chips (Chip-X) and the Yachen Foundation for their invaluable support.

Conflicts of Interest: The authors have no conflicts to disclose.

References

1. Gall, D.; Cha, J.J.; Chen, Z.; Han, H.-J.; Hinkle, C.; Robinson, J.A.; Sundararaman, R.; Torsi, R. Materials for Interconnects. *MRS Bull.* **2021**, *46*, 959–966. [CrossRef]
2. Witt, C.; Yeap, K.B.; Lesniewska, A.; Wan, D.; Jordan, N.; Ciofi, I.; Wu, C.; Tokei, Z. Testing The Limits of TaN Barrier Scaling. In Proceedings of the 2018 IEEE International Interconnect Technology Conference (IITC), IEEE, Santa Clara, CA, USA, 4–7 June 2018; pp. 54–56.
3. Wu, Z.; Li, R.; Xie, X.; Suen, W.; Tseng, J.; Bekiaris, N.; Vinnakota, R.; Kashefizadeh, K.; Naik, M. PVD-Treated ALD TaN for Cu Interconnect Extension to 5nm Node and Beyond. In Proceedings of the 2018 IEEE International Interconnect Technology Conference (IITC), IEEE, Santa Clara, CA, USA, 4–7 June 2018; pp. 149–151.
4. Kim, S.-H. Transmission Electron Microscopy Study of the Failure Mechanism of the Diffusion Barriers (TiN and TaN) between Al and Cu. *Met. Mater. Int.* **2017**, *23*, 141–147. [CrossRef]
5. Auger, M.A.; Gago, R.; Fernandez, M.; Sanchez, O.; Albella, J.M. Deposition of TiNyAlN Bilayers on a Rotating Substrate by Reactive Sputtering. *Surf. Coat. Technol.* **2002**, *157*, 26–33. [CrossRef]
6. Hu, Z.; Ren, L.; Zhao, K.; Wei, G.; Zhang, Z.; Han, T.; Zhong, F.; Yuan, M. A Novel Diffusion Barrier of Electrodeposited CoWP Layer between Copper and Silicon: Preparation and Performance. *Surf. Interfaces* **2022**, *30*, 101925. [CrossRef]
7. Lo, C.-L.; Catalano, M.; Smithe, K.K.H.; Wang, L.; Zhang, S.; Pop, E.; Kim, M.J.; Chen, Z. Studies of Two-Dimensional h-BN and MoS2 for Potential Diffusion Barrier Application in Copper Interconnect Technology. *Npj 2D Mater. Appl.* **2017**, *1*, 42. [CrossRef]
8. Nguyen, B.-S.; Lin, J.-F.; Perng, D.-C. Non-Vacuum Growth of Graphene Films Using Solid Carbon Source. *Appl. Phys. Lett.* **2015**, *106*, 221604. [CrossRef]
9. Deijkers, J.H.; De Jong, A.A.; Mattinen, M.J.; Schulpen, J.J.P.M.; Verheijen, M.A.; Sprey, H.; Maes, J.W.; Kessels, W.M.M.; Bol, A.A.; Mackus, A.J.M. MoS_2 Synthesized by Atomic Layer Deposition as Cu Diffusion Barrier. *Adv. Mater. Inter* **2023**, *10*, 2202426. [CrossRef]
10. Kang, Y.; Lee, S.; Choi, Y.; Seong, W.K.; Han, K.H.; Kim, J.H.; Kim, H.; Hong, S.; Lee, S.H.; Ruoff, R.S.; et al. Large-Area Uniform 1-nm-Level Amorphous Carbon Layers from 3D Conformal Polymer Brushes. A "Next-Generation" Cu Diffusion Barrier? *Adv. Mater.* **2022**, *34*, 2110454. [CrossRef]
11. Chang, S.-Y.; Li, C.-E.; Huang, Y.-C.; Hsu, H.-F.; Yeh, J.-W.; Lin, S.-J. Structural and Thermodynamic Factors of Suppressed Interdiffusion Kinetics in Multi-Component High-Entropy Materials. *Sci. Rep.* **2014**, *4*, 4162. [CrossRef]
12. Jang, Y.; Kim, J.B.; Hong, T.E.; Yeo, S.J.; Lee, S.; Jung, E.A.; Park, B.K.; Chung, T.-M.; Kim, C.G.; Lee, D.-J.; et al. Highly-Conformal Nanocrystalline Molybdenum Nitride Thin Films by Atomic Layer Deposition as a Diffusion Barrier against Cu. *J. Alloys Compd.* **2016**, *663*, 651–658. [CrossRef]
13. Hong, T.E.; Jung, J.-H.; Yeo, S.; Cheon, T.; Bae, S.I.; Kim, S.-H.; Yeo, S.J.; Kim, H.-S.; Chung, T.-M.; Park, B.K.; et al. Highly Conformal Amorphous W–Si–N Thin Films by Plasma-Enhanced Atomic Layer Deposition as a Diffusion Barrier for Cu Metallization. *J. Phys. Chem. C* **2015**, *119*, 1548–1556. [CrossRef]
14. Wang, W.-L.; Wang, C.-T.; Chen, W.-C.; Peng, K.-T.; Yeh, M.-H.; Kuo, H.-C.; Chien, H.-J.; Chuang, J.-C.; Ying, T.-H. The Reliability Improvement of Cu Interconnection by the Control of Crystallized α-Ta/TaNx Diffusion Barrier. *J. Nanomater.* **2015**, *2015*, 917935. [CrossRef]
15. Mahieu, S.; Depla, D. Reactive Sputter Deposition of TiN Layers: Modelling the Growth by Characterization of Particle Fluxes towards the Substrate. *J. Phys. D Appl. Phys.* **2009**, *42*, 053002. [CrossRef]
16. Chun, J.-S.; Carlsson, J.R.A.; Desjardins, P.; Bergstrom, D.B.; Petrov, I.; Greene, J.E.; Lavoie, C.; Cabral, C., Jr.; Hultman, L. Synchrotron X-ray Diffraction and Transmission Electron Microscopy Studies of Interfacial Reaction Paths and Kinetics during Annealing of Fully-002-Textured Al/TiN Bilayers. *J. Vac. Sci. Technol. A* **2001**, *19*, 182–191. [CrossRef]
17. Gall, D.; Kodambaka, S.; Wall, M.A.; Petrov, I.; Greene, J.E. Pathways of Atomistic Processes on TiN(001) and (111) Surfaces during Film Growth: An Ab Initio Study. *J. Appl. Phys.* **2003**, *93*, 9086–9094. [CrossRef]
18. Mahieu, S.; Ghekiere, P.; Depla, D.; De Gryse, R. Biaxial Alignment in Sputter Deposited Thin Films. *Thin Solid Film.* **2006**, *515*, 1229–1249. [CrossRef]
19. Arshi, N.; Lu, J.; Koo, B.H.; Lee, C.G.; Ahmed, F. Effect of Nitrogen Flow Rate on the Properties of TiN Film Deposited by e Beam Evaporation Technique. *Appl. Surf. Sci.* **2012**, *258*, 8498–8505. [CrossRef]
20. Shirley, D.A. High-Resolution X-ray Photoemission Spectrum of the Valence Bands of Gold. *Phys. Rev. B* **1972**, *5*, 4709–4714. [CrossRef]
21. Jaeger, D.; Patscheider, J. A Complete and Self-Consistent Evaluation of XPS Spectra of TiN. *J. Electron Spectrosc. Relat. Phenom.* **2012**, *185*, 523–534. [CrossRef]
22. Lou, H.Q.; Axén, N.; Somekh, R.E.; Hutchings, I.M. Effect of Deposition Conditions on the Characteristics of Reactively Sputtered Titanium Nitride Films. *Surf. Coat. Technol.* **1997**, *90*, 123–127. [CrossRef]
23. Greczynski, G.; Hultman, L. Self-Consistent Modelling of X-ray Photoelectron Spectra from Air-Exposed Polycrystalline TiN Thin Films. *Appl. Surf. Sci.* **2016**, *387*, 294–300. [CrossRef]
24. Van Der Straten, O.; Zhang, X.; Motoyama, K.; Penny, C.; Maniscalco, J.; Knupp, S. ALD and PVD Tantalum Nitride Barrier Resistivity and Their Significance in via Resistance Trends. *ECS Trans.* **2014**, *64*, 117–122. [CrossRef]

25. Bochkarev, A.S.; Popov, M.N.; Razumovskiy, V.I.; Spitaler, J.; Puschnig, P. Ab Initio Study of Cu Impurity Diffusion in Bulk TiN. *Phys. Rev. B* **2016**, *94*, 104303. [CrossRef]
26. Chowdhury, S.; Gupta, R.; Prakash, S.; Behera, L.; Phase, D.M.; Gupta, M. Synthesis and Study of Highly Dense and Smooth TiN Thin Films. *Mater. Chem. Phys.* **2021**, *267*, 124648. [CrossRef]
27. Piallat, F.; Gassilloud, R.; Caubet, P.; Vallée, C. Investigation of TiN Thin Film Oxidation Depending on the Substrate Temperature at Vacuum Break. *J. Vac. Sci. Technol. A Vac. Surf. Film.* **2016**, *34*, 051508. [CrossRef]
28. Liang, H.; Xu, J.; Zhou, D.; Sun, X.; Chu, S.; Bai, Y. Thickness Dependent Microstructural and Electrical Properties of TiN Thin Films Prepared by DC Reactive Magnetron Sputtering. *Ceram. Int.* **2016**, *42*, 2642–2647. [CrossRef]
29. Kearney, B.T.; Jugdersuren, B.; Culbertson, J.C.; Desario, P.A.; Liu, X. Substrate and Annealing Temperature Dependent Electrical Resistivity of Sputtered Titanium Nitride Thin Films. *Thin Solid Film.* **2018**, *661*, 78–83. [CrossRef]
30. Sondheimer, E.H. The Mean Free Path of Electrons in Metals. *Adv. Phys.* **2001**, *50*, 499–537. [CrossRef]
31. Cai, H.; Tong, D.; Wang, Y.; Song, X.; Ding, B. Reactive Synthesis of Porous Cu3Si Compound. *J. Alloys Compd.* **2011**, *509*, 1672–1676. [CrossRef]
32. Gao, W.; Belyakov, A.; Miura, H.; Sakai, T. Dynamic Recrystallization of Copper Polycrystals with Different Purities. *Mater. Sci. Eng. A* **1999**, *265*, 233–239. [CrossRef]
33. Nguyen, B.-S.; Lin, J.-F.; Perng, D.-C. 1-Nm-Thick Graphene Tri-Layer as the Ultimate Copper Diffusion Barrier. *Appl. Phys. Lett.* **2014**, *104*, 082105. [CrossRef]
34. Mühlbacher, M.; Greczynski, G.; Sartory, B.; Mendez-Martin, F.; Schalk, N.; Lu, J.; Hultman, L.; Mitterer, C. TiN Diffusion Barrier Failure by the Formation of Cu3Si Investigated by Electron Microscopy and Atom Probe Tomography. *J. Vac. Sci. Technol. B* **2016**, *34*, 022202. [CrossRef]
35. Lim, K.Y.; Lee, Y.S.; Chung, Y.D.; Lyo, I.W.; Whang, C.N.; Won, J.Y.; Kang, H.J. Grain Boundary Diffusion of Cu in TiN Film by X-ray Photoelectron Spectroscopy. *Appl. Phys. A Mater. Sci. Process.* **2000**, *70*, 431–434. [CrossRef]
36. Nazon, J.; Fraisse, B.; Sarradin, J.; Fries, S.G.; Tedenac, J.C.; Fréty, N. Copper Diffusion in TaN-Based Thin Layers. *Appl. Surf. Sci.* **2008**, *254*, 5670–5674. [CrossRef]
37. Chen, S.-F.; Wang, S.-J.; Yang, T.-H.; Yang, Z.-D.; Bor, H.-Y.; Wei, C.-N. Effect of Nitrogen Flow Rate on TaN Diffusion Barrier Layer Deposited between a Cu Layer and a Si-Based Substrate. *Ceram. Int.* **2017**, *43*, 12505–12510. [CrossRef]